LoSense: Integrated Long-Range Sensing and Communication with LoRa Signals

Zhipeng Song, Shuai Tong, Jiliang Wang

School of Software, Tsinghua University, Beijing, China

{songzp18,tl19}@mails.tsinghua.edu.cn,jiliangwang@tsinghua.edu.cn

Abstract—As a representative Low Power Wide Area Network (LPWAN) technology, LoRa is expected to connect devices for various Internet of Things (IoT) applications. Many IoT applications require both long-range communications and high precise sensing at the same time, while state of the art approaches fail to achieve this. We propose *LoSense*, which enables LoRa movement sensing alongside the regular data transmissions. *LoSense* recovers the fine-grained trajectory of a LoRa transmitter only based on its communication signals during the data transmission period. We address practical challenges for *LoSense* designs. We propose the active tracking model for detecting movements of active LoRa transmitters. We use dual antennas at the receiver to eliminate synchronization offsets between LoRa transmitters and the receiver. We design feature amplification and signal enhancement schemes to combat noise and interference. We prototype *LoSense* with commodity LoRa transmitters and USRP receivers, and extensively evaluate its performance. The results show that *LoSense* tracks movements of active LoRa transmitters with 2.32 cm distance accuracy and 0.089 Hz frequency accuracy from a sensing range of 150m, supporting regular data communication at the same time.

I. INTRODUCTION

As a promising Low Power Wide Area Network (LPWAN) technique, LoRa is expected to provide services for various Internet of Things (IoT) applications such as smart agriculture [1], industrial automation [2], supply chain management [3], etc. Many IoT applications require both high performance sensing and wireless communications. For example, in the drone navigation system, the controller needs to track the real-time movement of the drone during its data communication. Therefore, the controller can dynamically adjust the communication parameters, such as the transmitting power and coding rates, according to the orientation and distance changes of the drone. Most existing sensing and communication systems are designed separately and operate in isolated frequency bands. This leads to more competition on the scarce wireless spectrum and also increases the power consumption of end devices. In this paper, we ask the question - "Can we achieve simultaneous long-range sensing and communication on low-cost IoT devices by analyzing patterns and characteristics of LoRa signals?"

The main advantages of LoRa are low power consumption and long communication range. A typical LoRa device with the LoRaWAN protocol can communicate over several kilometers, and has a battery life for nearly 10 years [4]. These properties make LoRa feasible to cover a large area with a low deployment cost. Owing to the wide coverage and low deployment cost, much research has been proposed for exploring the sensing ability of LoRa signals. These works can be classified into two categories: *1) Localization.* Many research works focus on obtaining the location information by exchanging signals between active LoRa devices or passive backscatter tags. Typical techniques for LoRa localization involves Time Difference of Arrival (TDoA) [5]–[7], Received Signal Strength Indicator (RSSI) [8], [9], phase or Channel State Information (CSI) [10], [11], and fingerprinting [12]. The LoRa localization approaches require packets exchanging between multiple devices and take a long processing time. Therefore, they cannot support real-time movement tracking applications. *2) Passive tracking.* Recent literatures propose passive tracking by analyzing RF signals reflected by target objects. These techniques are usually used to detect human activities, such as breathing, heart beating, and walking [13]–[15]. However, the passive tracking requires the transmitters to generate signals in specific forms, and cannot support communicate simultaneously with sensing.

Fundamental limitations. All previous LoRa sensing techniques require dedicated signals with known frequencies and phases. They cannot perform wireless sensing alongside communication signals. Thus, these systems are not suitable for low-cost and low-power LoRa, as they increase the spectrum occupation and burden the node energy consumption with separated sensing and communication systems.

Limitations of previous research motivate us to rethink the design LoRa sensing methods. We propose *LoSense*, a high-precise LoRa sensing technique that tracks the movement of LoRa devices alongside its normal data communication. Instead of providing absolute position tracking in continuous time, *LoSense* senses the relative movement of a device during each of its intermittent transmissions. *LoSense* is useful in many IoT applications that need movement tracking at the same time of data communication. For example, in the scenario of wireless communication with moving devices, e.g., drones and boats, the network controller can adopt the *LoSense* movement tracking for dynamically adjusting the transmission parameters, e.g., coding rate and transmitting power, or scheduling perfect time for the next transmission. Previous literatures show the effectiveness of using the information of transmitter movements for improving the communication performance [16]. To track the movement of LoRa nodes, *LoSense* exploits to extract the phase information from low-

SNR LoRa signals. We implement *LoSense* with commodity LoRa transmitters and USRP receivers without hardware modification on the LoRa node. Therefore, *LoSense* can be easily applied on existing LoRa devices.

Taking the idea of *LoSense* into practice, however, still faces challenges: *1) How to build the tracking model for low-power active LoRa devices:* Previous wireless tracking with the passive signal reflection is inapplicable for LoRa device tracking with active communication signals. We propose a dual-antenna receiver based tracking model that uses an idle node in the same network as the helper node for detecting the movement of the target transmitter. *2) No clock synchronization:* LoRa does not provide synchronization between end nodes and gateways, which leads to carrier frequency offsets and sample frequency offsets in the received signal. Extracting clean phases for device tracking with such signals can be very challenging. We propose the offset elimination strategy with the dual-antenna receiver to solve the synchronization problem. *3) Tracking against noise and interference:* Long-range communication with strong signal attenuation and interference results in LoRa signals below the noise floor. We propose a signal enhancement method by energy accumulation and outliers elimination to extract signal features against strong noise and interference.

We implement *LoSense* with LoRa transmitters and USRP receivers, and conduct extensive experiments to evaluate its performance. Our results show that *LoSense* achieves long-range and high-precise active device tracking while supporting data communications. In summary, our contributions are as follows:

- We propose *LoSense*, an active tracking system that integrated long-range sensing and data communication at the same time.
- We analyze the active tracking model for LoRa signals. We address the synchronization offsets between LoRa devices by introducing the dual-antenna receiver. We propose the anti-noise design with energy accumulation and outlier elimination that enables accurate LoRa tracking with extremely low-SNR signals.
- We implement *LoSense* with COTS LoRa transmitter and USRP software defined radios. We carry out extensive experiments to evaluate its performance in both indoor and outdoor scenarios. The results show that *LoSense* tracking achieves 2.32cm distance accuracy and 0.089Hz frequency accuracy at the sensing range of 150m and supports regular data communication at the same time.

The rest of the paper is organized as follows: §2 introduces the preliminaries of LoRa. §3 discusses realistic requirements for applying long-range sensing in LoRa. We present the active tracking model in §4 and the combating noise design in §5. §6 presents implementation details and §7 shows evaluation results. §8 discusses the related works. We conclude *LoSense* and discuss future works in §9.
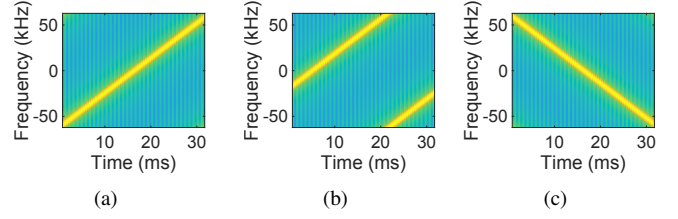

Fig. 1. Spectrogram of LoRa physical layer signals: (a) an up-chirp with increasing frequencies; (b) an encoded chirp with the shifted initial frequency; (c) a down-chirp with decreasing frequencies

II. LoRa Primer

LoRa PHY. LoRa leverages Chirp Spreading Spectrum (CSS) at the physical layer, where signals are modulated into chirps whose frequencies change linearly with time. Key parameters for LoRa chirp modulation include *bandwidth* (BW), and *spreading factor* (SF), which determine data rates of LoRa transmissions. Thus, a chirp symbol can be mathematically represented as:

$$C(t) = e^{j2\pi(-\frac{BW}{2}t + \frac{k}{2}t^2)}, \quad 0 \le t < T \qquad (1)$$

where $T = 2^{SF}/BW$ is the duration of a chirp, and $k = BW/T$ is the slope of the varying frequency over time. A chirp with a positive k has the frequency increasing with time, which is named *up-chirp* as shown in Figure. 1(a). On the contrary, a chirp with decreasing frequencies is named *down-chirp* as shown in Figure. 1(c). Both the *up-chirp* and the *down-chirp* are used in the LoRa preamble for packet synchronization at the receiver. LoRa modulates data bits by cyclically shifting the initial frequency of up-chirp, as shown in Figure 1(b).

Packet structure. A LoRa packet is composed of a preamble, an optional header, a payload and a two-byte CRC calculated from the payload data. The preamble consists of a varied number of base chirps, followed by a two-chirp synchronization word and 2.25 down chirps as a Start Frame Delimiter (SFD). A LoRa radio detects a packet by detecting the presence of LoRa preamble and uses the preamble for frame synchronization. Upon detecting a preamble, a receiver detects SFD to identify the start of payload and next demodulate and decode the payload. The CRC will be checked by a receiver to validate the integrity of received data.

ISAC in LoRa. Much recent research pays close attention to the integrated sensing and communication (ISAC) [17], [18] which enables the entire communications network to serve as a sensor. With ISAC, we can sense the device movement alongside the LoRa communication signals. The radio wave transmissions, reflections, and scattering can be used to sense and better understand the motion state of LoRa devices. Meanwhile, we can adjust the LoRa parameters, such as the physical layer data rate and the antenna orientation, according to the real-time motion state of the transmitter, to optimize the network transmission performance.
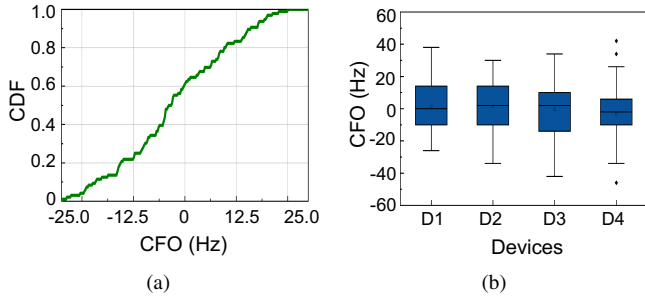
Fig. 2. CFO fluctuation: (a) CFO on a single transmitter over one-minute transmissions, (b) CFO variation for different hardwares.

III. REQUIREMENTS FOR LoRa SENSING

There are several realistic requirements we have to meet for applying the long-range sensing in LoRa.

(i) CFO elimination: We sense the movement of a LoRa transmitter by extracting the motion-related phase from its communication signals. However, the oscillators of low-cost LoRa nodes are usually unsynchronized, leading to carrier frequency offsets (CFO) between the transmitter and receiver. The CFO introduces a time-varying phase in the received signal, which is confused with the movement-induced phase change, leading tracking errors. To accurately sense the movement of a LoRa transmitter, we have to eliminate the impact of the CFO on phase tracing of the received signal. We propose a two-antenna receiving model to remove impacts of the time-varying CFO on the received signal.

(ii) Feature amplification: In the far-field LoRa networks, the distance of device movement is much less than the communication ranges. The phase features by the transmitter movement are inconspicuous at the receiver. For high-sensitive movement tracking, we have to amplify the phase features for the received signal. We introduce an idle node in the same network as the helper transmitter that sends LoRa signals alongside the target node. Signals of the two nodes superpose over the air, leading to amplification of phase variation at the receiver. We propose a complete theoretical proof to show why the helper node can amplify the phase features in § IV-B. A node can act as a helper as long as it is static and its signal can reach the same receiver as the target node. Thus, one helper node can serve a large number of other nodes in the same network, making *LoSense* scalable.

(iii) Sensing bellow the noise floor: The SNR of LoRa can be below the noise floor due to long-range communication with strong signal attenuation, interference and complex multi-path. For tracking the movement of long-range LoRa transmitters, we propose signal enhancement method to extract signal features even bellow the noise floor. We analyze the impact of signal multi-path in LoRa movement tracking, and propose a realistic method to eliminate its influence by adjusting the orientation of receiving antennas.

IV. TRACKING MODEL

A. Phase Variation Detection

We track the movement of a LoRa node by detecting the phase variation of its transmitted signal. Intuitively, we can track the distance between the transmitter and the receiver by detecting the phase variation with a single receiving antenna, as shown in Figure 3(a). Considering a signal $s(t)$ is transmitted over a single Line-of-Sight (LOS) path, the received signal becomes

$$R(t) = a \cdot s(t) \cdot e^{-j\frac{2\pi d(t)}{\lambda}} \tag{2}$$

where a is the signal attenuation, λ is the wave length, and $d(t)$ is the propagation distance that varies over time.

Theoretically, the distance variation between the transmitter and the receiver (i.e., $d(t)$) can be estimated by extracting the path-induced phase from the received signal. However, in practice, the local oscillators of the transmitter and the receiver are unsynchronized, inducing a Carrier Frequency Offset (CFO) between the two devices. Therefore, the received signal becomes

$$R(t) = a \cdot s(t) \cdot e^{-j\frac{2\pi d(t)}{\lambda} + 2\pi\Delta ft}$$

where $2\pi\Delta ft$ is the phase variation introduced by the CFO. To extract the distance-related phase vibration, we have to eliminate the effect of the CFO.

Previous work proposes to combat the CFO-induced phase error by measuring the CFO beforehand and calibrating it in the phase tracking [15]. Such an idea, however, has significant cumulative errors in long-term tracking, as the CFO has incapable jitter in long run. Its effect on phase variation is coupled with that induced by Tx's vibration, therefore it's difficult to calibrate the error caused by CFO in long run. Figure 2 shows the CFO jitter between commodity LoRa transmitters and a USRP receiver. we set two stationary USRP N210 as Tx and Rx, separated by 1 meter, and observe the CFO change within 1 minute. The result is shown in Figure 2(b). We configure each transmitter to send 50 LoRa packets in one minute and estimate the CFO in each received packet. Our evaluation on real LoRa transmitters shows that the CFO of a single device varies about 50 Hz in one minute, which introduces phase errors up to 1.89×10^4 rad, corresponding to a distance error of 9.83 m.

To combat the challenge of synchronization between the LoRa transmitter and receiver, we use a dual-antenna receiver for phase detection. As shown in Figure 3(b), the receiver is equipped with two antennas that share the same clock. Denote the transmitted signal as $s(t)$, the propagation distance to the two antennas are $d_1(t)$ and $d_2(t)$, respectively. We model the received signal at the two antennas as:

$$R_i(t) = a_i e^{-j\frac{2\pi d_i(t)}{\lambda} + \Delta ft} * s(t) = D_i(t)s(t), i = 1, 2 \tag{3}$$

where $D_1(t)$ and $D_2(t)$ denotes the dynamic channel between the transmitter and the two receiving antennas. Both $D_1(t)$ and $D_2(t)$ are related to the CFO between the transmitter and
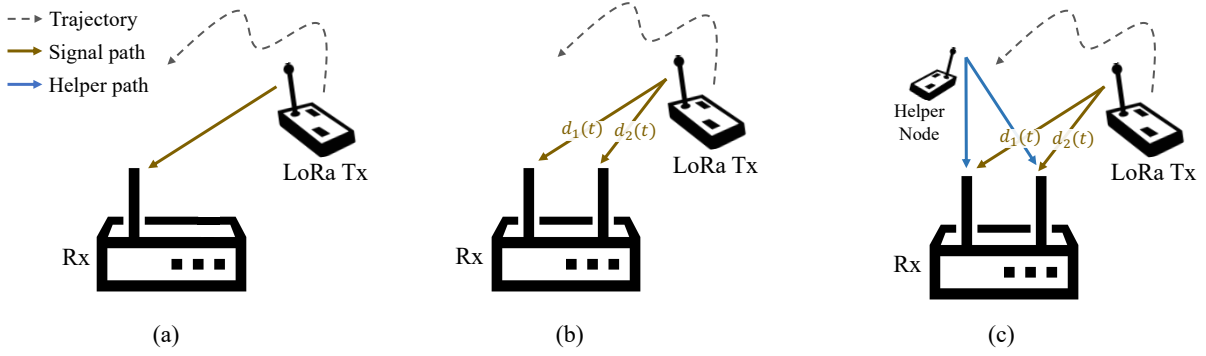
Fig. 3. Models for active sensing: (a) single-antenna model; (b) dual-antenna model; (c) *LoSense* with concurrent transmissions from a helper node.

the receiver. Therefore, we eliminate the impact of CFO by dividing $R_1(t)$ by $R_2(t)$, and finally obtain the signal ratio $SR(t)$ as

$$SR(t) = \frac{R_1(t)}{R_2(t)} = \frac{D_1(t)}{D_2(t)} = \frac{a_1}{a_2} \cdot e^{-j\frac{2\pi}{\lambda}(d_1(t)-d_2(t))} \quad (4)$$

Through the signal dividing, phase errors introduced by the CFO are all canceled out. The phase of the $SR(t)$ is only related to the path difference of the two receiving antennas. Thus, we can estimate the movement of the signal transmitter by detecting the phase variation of $SR(t)$.

B. Phase Feature Amplification

Now, we have eliminated the CFO impact in the received signal. We then detect the movement induced phase variation from the signal ratio $SR(t)$. In the real-world deployment, the signal paths to the two receiving antennas can be very similar, resulting in very small phase variations corresponding to path differences (i.e., $d_1(t)$ is similar to $d_2(t)$). To accurately recover the phase variation of $SR(t)$, we have to amplify the phase features of the received signal.

We first explain why the phase variation of $SR(t)$ is diminutive and difficult to detect. For theoretical illustration, we set both the transmitter and the dual-antenna receiver in a Cartesian coordinate system, as shown in Figure 4. The distance between the two receiving antennas is d, and the initial position of the transmitter is $P : (l\cos\theta, l\sin\theta)$, where l is distance between P and the origin point, and θ is the polar angle of P to the positive X-axis.

We stipulate the maximum moving range of the transmitter along the direction from the origin to P is A. In the far-field tracking scenario, we can assume that the spacing of the two receiving antennas and the device movement range is much smaller than the distance between the transmitter and the receiver, i.e., $l >> A$ and $l >> d$.

Therefore, the path difference to the two receiving antennas for the transmitter at P_1 becomes

$$\Delta s^{(1)} \approx d\cos\theta_1 \approx \frac{d^2}{l - \frac{A}{2}} \quad (5)$$

Similarly, the path difference when the transmitter is at position P_2 can be presented as $\Delta s^{(2)} \approx \frac{d^2}{l + \frac{A}{2}}$. Given the maximum moving range A of the transmitter, the path difference for the two receiving antennas is in a range of $[\Delta s^{(2)}, \Delta s^{(1)}]$. Thus, the maximum phase variation of $SR(t)$ is calculated as

$$\max \Delta\varphi_{SR} = \frac{2\pi}{\lambda}(\Delta s^{(1)} - \Delta s^{(2)}) \approx \frac{2\pi}{\lambda}\frac{d^2}{l^2}A \quad (6)$$

Eq. 6 shows that the phase variation of $SR(t)$ is very small in the far-field scenario, which tends to be masked in noise, causing high errors in phase tracking.

We introduce a static helper node for amplifying the phase features, as shown in Figure 3(c). For effective feature amplification, the signals of the helper node should arrive at the receiver almost simultaneously as the target node with the same content. The helper node and the target node does not need to be physically adjacent. To promise that the helper node sends the desired synchronized signal, we present a time and frequency synchronization scheme, where a LoRa gateway broadcasts beacons and the helper node adjusts its time and carrier frequency based on the reception.

Denote the static channel between helper node and two receiving antennas as S_1 and S_2 respectively, then the received signal of the two antennas becomes

$$R_i(t) = S_i s(t) + D_i(t)s(t), i = 1, 2 \quad (7)$$

The ratio of these two signals becomes

$$SR(t) = \frac{R_1(t)}{R_2(t)} = \frac{S_1 + a_1 e^{-j\frac{2\pi d_1(t)}{\lambda}}}{S_2 + a_2 e^{-j\frac{2\pi d_2(t)}{\lambda}}} \quad (8)$$

Previously, we have proved that the path difference of $d_1(t)$ and $d_2(t)$ is almost unchanged in the far-field scenario. Thus, we denote $d_1(t)$ as $d_2(t)$ minus a constant value Δs. To simplify Equation 8, we define four constants as follows:

$$a := a_1 e^{-j\frac{2\pi\Delta s}{\lambda}}, b := S_1, c := a_2, d := S_2, \eta(t) = e^{-j\frac{2\pi d_2(t)}{\lambda}}$$

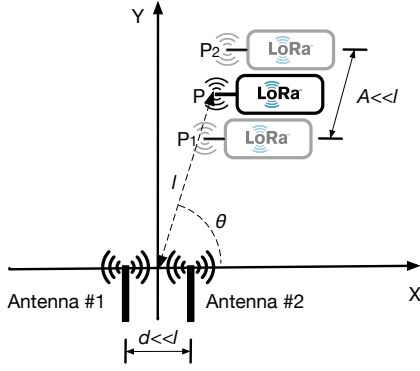Then, we plug the four values into Eq 8 and transform the equation into a simplified form as

Fig. 4. Theoretical model for the dual-antenna receiver in a Cartesian coordinate system.

Fig. 5. Phase feature amplification by samples transformation in the I/Q plane

$$SR(t) = \frac{b + a\eta(t)}{d + c\eta(t)} = \frac{bc - ad}{c} \frac{1}{c\eta(t) + d} + \frac{a}{c} \quad (9)$$

In the complex plane, η forms an arc if the variation of $d_2(t)$ is less than a wavelength, as shown in Figure 5. The phase change of this arc represents the change of $d_2(t)$, containing the moving distance of the target.

The $SR(t)$ in Eq. 9 applies rotation (multiplication), transformation (addition) and inversion to the arc $\eta(t)$. Essentially all the above can be treat as Möbius Transformation [19], which only changes an arc's position and size, but keeps its shape (i.e., α and β are equal in Figure 5). Therefore, we can recover $d_2(t)$ by estimating the central angle of the amplified curve (i.e., β) in the I/Q plane.

To show the effectiveness of the phase feature amplification, we revisit the example in Figure 4. When the transmitter is at point P_1, denote the path length between the transmitter and the first receiving antenna is $d_1^{(1)}$. When the transmitter is at point P_2, the corresponding length is $d_1^{(2)}$. The maximum phase variation of $SR(t)$ now becomes

$$\frac{2\pi}{\lambda}(d_1^{(2)} - d_1^{(1)}) == \frac{2\pi}{\lambda}((l + \frac{A}{2}) - (l - \frac{A}{2})) = \frac{2\pi}{\lambda}A \quad (10)$$

Comparing Eq. 10 with Eq. 6, by introducing a static neighbor node, we amplify the phase variation of signal ratio $SR(t)$ from $\frac{2\pi}{\lambda}\frac{d^2}{l^2} \cdot A$ to $\frac{2\pi}{\lambda} \cdot A$.

C. Trajectory Extraction

This section describes how to extract the trajectory of the transmitter from the extracted phase features. We first focus on one-dimensional distance tracking. As described in Sec. IV-B, by dividing the signals received at the two antennas, we obtain an arc-shaped curve $SR(t)$. As shown in Figure 5, the Möbius transformation keeps the central angle of the arc (i.e., $\alpha = \beta$). Therefore, we can compute the central angle of $SR(t)$ and get the phase variation of $\eta(t)$. Assume the target starts moving at time t_1 and stops at time t_2, taking $\eta(t) = e^{-j\frac{2\pi d_2(t)}{\lambda}}$ into consideration, we can obtain the moving distance:
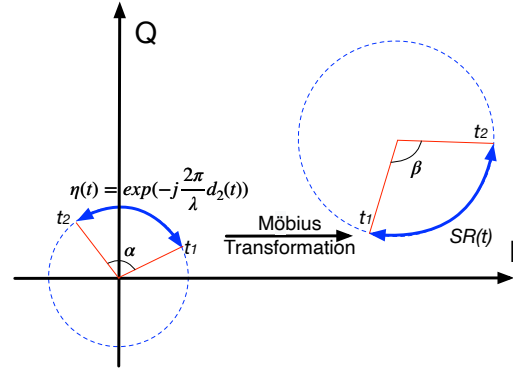
$$d_2(t_2) - d_2(t_1) = \frac{\lambda}{2\pi}(\angle\eta(t_2) - \angle\eta(t_1)) = \frac{\lambda}{2\pi}\alpha \quad (11)$$

When time period between t_1 and t_2 approaches to zero, we can obtain the instantaneous movement and directional speed of the transmitter, i.e., the trajectory of the device in one dimension direction. Further, if the transmitter moves periodically, e.g., vibration, we can recover the frequency of the movement. To achieve this, we perform the Fast Fourier Transform (FFT) on signal ratio samples, i.e., $SR(t)$ in Eq. 9. Then, we extract the highest peak from the Fourier transform output, where the index of the peak reflects the frequency of the periodical movement. To track the transmitter in a 2-dimension plane, we need at least two receivers to track the movement of the transmitter in two different directions. We extract one-dimension trajectory from the two receivers, respectively. Then, giving the movement along the two directions, we can apply a geometry model described in [20] to track the 2-D trajectory of the transmitter.

V. DEAL WITH LOW-SNR LORA SIGNAL

A. Energy Accumulation

We propose an energy accumulation strategy to combat the impact of channel noise. Our key observation is that the energy of a whole chirp can be accumulated for estimating its initial phase. As shown in Figure 6, the received chirp $R(t)$ falls into a decoding window. We denote the phase of the beginning sample in this window as the *initial phase*. We apply the FFT on the dechirped signal, which results in both an amplitude spectrum and a phase spectrum in the frequency domain. The peak position of the amplitude spectrum has its counterpart in the phase spectrum, whose value is the *initial phase* of signals in that window.

We now illustrate why the value in the phase spectrum is the *initial phase* of the corresponding signal. Assume the initial phase of $R(t)$ in the decoding window is ϕ. For signal in the decoding windows, we perform *dechirp* by multiplying the signal with a standard down-chirp whose initial phase is 0. After *dechirp*, we obtain a single-tone signal $D(t)$ whose initial phase is ϕ, i.e., $D(t) = e^{j2\pi f_c t + \phi}$. Then, we perform
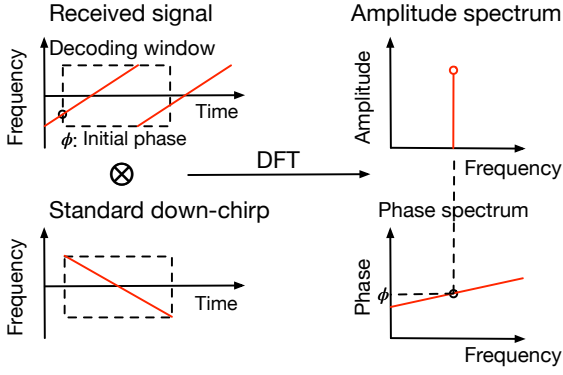
Fig. 6. Energy accumulation for phase extraction.

Fig. 7. Outlier elimination based circle fitting for samples in the I/Q plane.

Algorithm 1 Outliers Elimination

Input :
    n signal ratio I/Q samples $s[1], s[2], \cdots, s[n]$

Output :
    n outlier-eliminated samples $s'[1], s'[2], \cdots, s'[n]$

 1: $s'[1] \Leftarrow s[1]$
 2: $s'[n] \Leftarrow s[n]$
 3: **for** each $i \in [2, n-1]$ **do**
 4:    **if** $abs(angle(s[i]) - angle(s'[i-1])) \geq \frac{\pi}{2}$ **then**
 5:       $\theta = (angle(s'[i-1]) + angle(s[i+1]))/2$
 6:       $s'[i] \Leftarrow abs(s[i]) * e^{j\theta}$
 7:    **else**
 8:       $s'[i] \Leftarrow s[i]$
 9:    **end if**
10: **end for**

FFT on $D(t)$ to transform the signal from time domain to the frequency domain as follows

$$\mathcal{F}(f) = \sum_{n=0}^{N-1} D(\frac{n}{N}T)e^{-j2\pi fn} = \sum_{n=0}^{N-1} e^{j2\pi(\frac{T}{N}f_c - f)n + \phi} \quad (12)$$

We detect the energy peak from the FFT output as $|\mathcal{F}(\frac{T}{N}f_c)|$. Its counterpart in the phase spectrum $\angle\left(\mathcal{F}(\frac{T}{N}f_c)\right) = \phi$ is exact the initial phase of $R(t)$ in the time domain. By energy accumulation, we leverage the information of all samples in a chirp as in Eq. 12. Therefore, the estimated phase values are more robust to channel noises compared to directly using initial phase from the time domain. This idea requires the movement distance between two adjacent chirps no longer than a wavelength. For nodes moving with a high speed, we can shorten the chirp duration by using higher bandwidth or lower SF. Besides, we can also use short windows for energy concentration, e.g., using windows of half a chirp, thus to tracking targets with high-speed movements.

From the scheme above, we can see As long as the node movement does not exceed half of the wavelength within a chirp duration, our system will work well for multiple wavelength. We obtain a tracking sample by concentrating the energy of a whole LoRa chirp. For nodes moving with
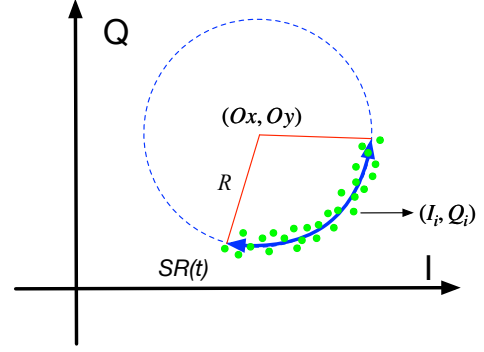
a high speed, we can shorten the chirp duration to improve the sampling rate for movement tracking, and to achieve this we can use higher bandwidth or lower SF. Apart from that, we can also use short windows for energy concentration, e.g., using windows of half a chirp, thus to achieve higher sampling rates for high-speed movements.

B. Alleviate the Impact of Noise

Ideally, after energy accumulation, the resulted $SR(t)$ should be a series of samples that has continuous phases in the I/Q plane, as shown in Figure 5. In practice, there are outliers far from the ideal arc due to the channel noise, as shown in Figure 7. To tackle with this problem, we apply a time-ordered sample filtering strategy, as described in Algorithm 1. This algorithm takes signal ratio samples (i.e., $SR(t)$) as the input, and output a sequence of outlier-eliminated samples. The key idea of the algorithm is to identify and remove outlier samples by comparing the phases for each pair of adjacent samples. The $angle$ function in the algorithm computes the *unwrapped phase*, which means the difference of computed phases for two adjacent samples should be less than π.

In addition to the outliers detection and elimination, we further propose a circle fitting scheme to reduce the residual impacts of channel noise. Denote the ideal circle has the center coordinate of (Ox, Oy), and a radius of R. The samples from the outlier eliminate algorithm output is $I_1, I_2, \cdots, I_n$ and $Q_1, Q_2, \cdots, Q_n$. To fit these samples on the ideal circle, we have to solve the following problem

$$\min_{\{Ox,Oy,R\}} \{\sum_{i=1}^{n}(dist[(Ox, Oy), (I_i, Q_i)]^2 - R^2)^2\}$$
$$= \min_{\{Ox,Oy,R\}} \{\sum_{i=1}^{n}[(Ox - I_i)^2 + (Oy - Q_i)^2 - R^2]^2\} \quad (13)$$

where $dist(P_1, P_2)$ denotes the 2-D Euclidian distance between two points P_1 and P_2. We leverage a Matlab function $nlinfit$ [21] for this non-linear regression problem, and thus reduce the impact of random I/Q shifts on *LoSense*.
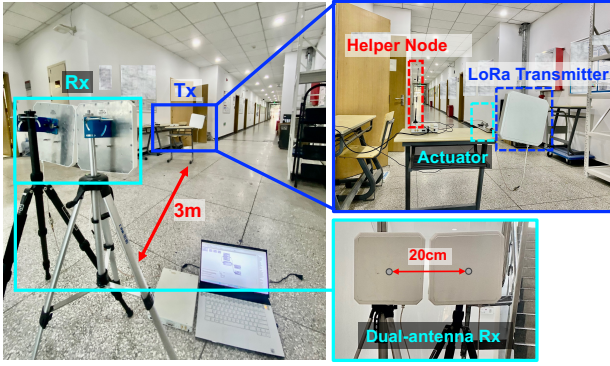
Fig. 8. Indoor experiment settings in the hallway of an office building.

VI. IMPLEMENTATION

We prototype *LoSense* with a moving LoRa transmitter, a static helper node, and a two-antenna receiver. We perform one-dimensional distance tracking in the evaluation with a single receiver. Position tracking in 2D or 3D space can be achieved by using multiple receivers as described in Sec. IV-C. The *LoSense* transmitter and the helper node are implemented on COTS LoRa nodes with SX1276 [22] that send standard LoRa packets continuously. The receiver is implemented with the USRP X310 software defined radio, which has two separate radio front ends sharing the same clock. The USRP at the receiver is connected to a PC with an Intel Core i9-12900H CPU and 16GB RAM via Ethernet cables, which collects and demodulates physical samples of arrived LoRa packets. We use the collected signal samples for tracking the distance variation from the transmitter and evaluating fine-grained distance and frequency tracking errors. Both the *LoSense* transmitter and receiver use Laird S9028PCR directional antennas with a 9 dB gain. The helper node uses an omni-directional antenna with a 2 dB gain. For component-level evaluation, we implement a *LoSense* transmitter on a USRP N210 software defined radio and connect the helper node to the *LoSense* transmitter via a splitter to promise that both the two transmitters send the same signal. We employ UHD + GNU-Radio library [23] to generate LoRa signals, and use MATLAB to process received samples. It should be noted that *LoSense* can be totally implemented in COTS LoRa transmitters instead of the USRP. The implementation on USRP is mainly for micro-benchmarks evaluation.

We evaluate *LoSense* with both an indoor testbed and a campus-scale testbed. During the distance tracking, we demodulate every LoRa packet at the receiver and evaluate both packet delivery rates and bit error rates for showing the impact of device tracking on communication. Unless specified otherwise, packets in our evaluations are generated with SF12, 125 kHz bandwidth and 915 MHz carrier.

VII. EVALUATION

A. Benchmark Experiment

In this experiment, we evaluate the accuracy of *LoSense* in terms of distance tracking and the period of target motion

under various LoRa configurations.

Experiment setting: We perform the benchmark experiment with an indoor testbed where the transmitter and the receiver are separated by 3m, as shown in Figure 8. We install the antenna of the *LoSense* transmitter on a reciprocating linear actuator, and make it reciprocate at a period of 2 seconds (i.e., 0.5 Hz) with a maximum moving range of 15 cm. We place the helper node near the transmitter and keep its antenna static. Both the *LoSense* transmitter and the helper node transmit the same LoRa packets continuously. We conduct the experiment under various LoRa configurations with SF from 7 to 12 and BW amongst 125 kHz, 250 kHz, and 500 kHz. For each configuration, we make the transmitter generate twenty rounds of transmissions. In each round, we compute the distance and frequency of the device's reciprocating movement based on the tracking model in Sec. IV. Furthermore, we evaluate the performance of *LoSense* in low-SNR scenarios. For the received signal of each LoRa configuration, we add white Gaussian noise to generate LoRa transmissions with various SNRs.

Results: Figure 9 shows the distance tracking errors under various LoRa configurations and SNRs. The distance tracking errors are estimated by comparing the tracked distance variation with the actual moving range. As shown in Figure 9(a), the tracking errors of *LoSense* increase as the SNR decreases with all SF configurations. This is due to the channel noise that impacts phase feature extraction for *LoSense* tracking. Even though, *LoSense* can achieve high-precise tracking even when transmissions are under the noise floor. This is because the combating noise designs in the *LoSense* architecture, where we concentrate the energy of LoRa chirps in the time domain and eliminate outliers for circle fitting. The averaged distance tracking error is only 0.05m for LoRa SF 7 under an SNR of -5 dB, and the error is less than 0.1m for LoRa SF 12 with an SNR of -25 dB. Then, we exploring the relationship between tracking accuracy with the signal bandwidth by comparing the results in Figure 9(a), (b), and (c). We have illustrated in Sec. II that the duration of a LoRa chirp is related to the bandwidth configuration, where a lower BW leads to a longer LoRa chirp. Therefore, *LoSense* achieves the best tracking accuracy when BW is 125 kHz, where the averaged tracking error is 7.34 cm for -25 dB SNR.

Further, we examine the accuracy of *LoSense* in tracking the frequency of the device movement. The frequency error is estimated by comparing the tracked device moving frequency with the actual frequency of the actuator motion (i.e., 0.5 Hz). Frequency tracking fails when there is no prominent FFT peak as described in Sec. IV-C. We omit the tracking failures and calculate the averaged frequency error for each configuration under various SNR settings. Figure 10(a) shows frequency error over different SFs given the bandwidth fixed at 125 kHz. *LoSense* achieves precise frequency tracking even under extremely low SNR, e.g., the frequency error is only 0.02 Hz under the SNR of -10 dB with SF7.

The SNR requirement for frequency tracking is much easier than the distance tracking. For frequency analysis, we gather
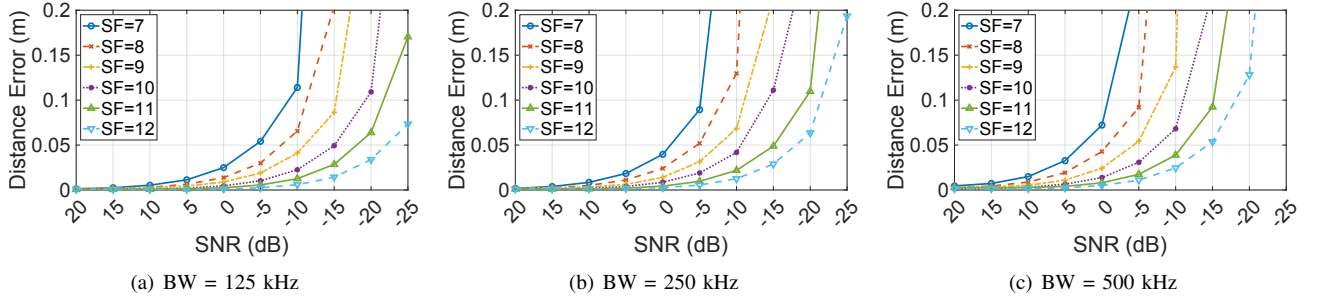
Fig. 9. Distance tracking errors under different LoRa transmission configurations and various SNRs.
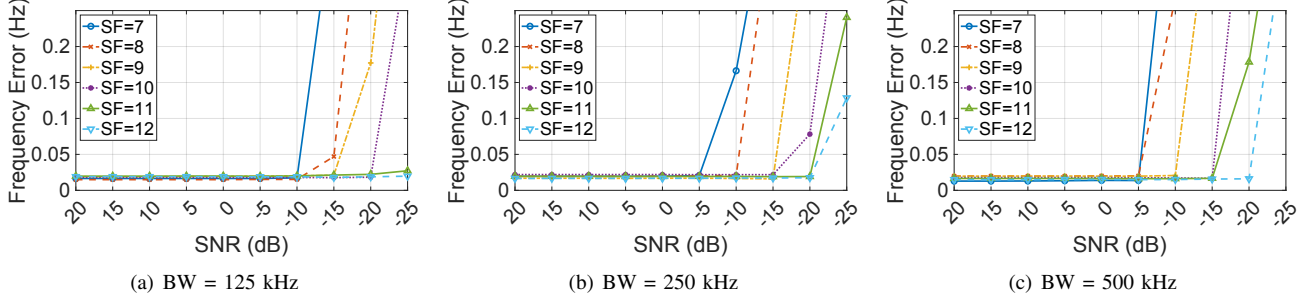

Fig. 10. Frequency tracking errors under different LoRa transmission configurations and with various SNRs.
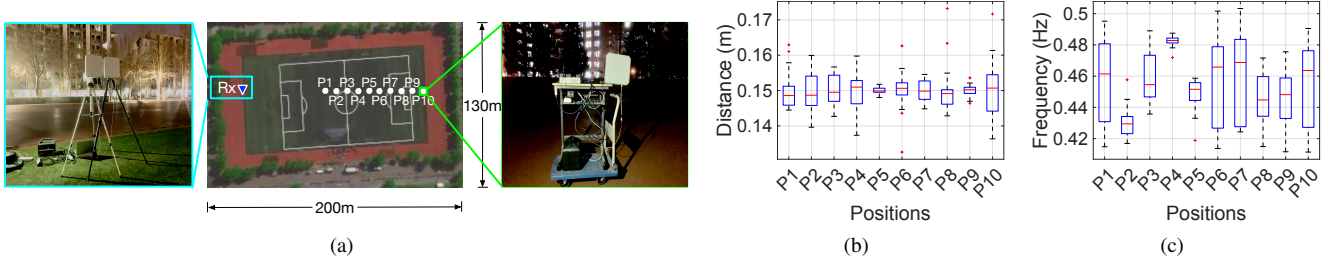

Fig. 11. Outdoor long-range active tracking: (a) A bird view of the experiment area and the setup of the LoRa transmitter and *LoSense* receiver; (b) Distance tracking errors at different positions; (c) Frequency tracking errors.

the energy of all samples in the estimation period by FFT, which is resistant to outlier samples. However, for distance tracking, a single outlier sample can introduce significant errors in circle fitting. We also evaluate frequency errors over various bandwidth configurations. The results are shown in Figure 10, where signals with lower bandwidth have longer chirp durations and thus have better tracking performance. To summarize, *LoSense* achieves as low as 0.02 Hz frequency tracking error even under -25 dB SNR given a suitable LoRa configuration.

B. Component-level Evaluation

Experiment setting: In this experiment, we validate two key parts of the *LoSense* design, i.e., the helper node and the energy accumulation. We rule each part out of our system and build two systems as elaborated below:

(1) LoSense W/O helper node: We build this system by keeping the helper node stay in silence. According to Sec. IV-B, without the helper node, *LoSense* cannot amplify the phase difference of signals received by two antennas.
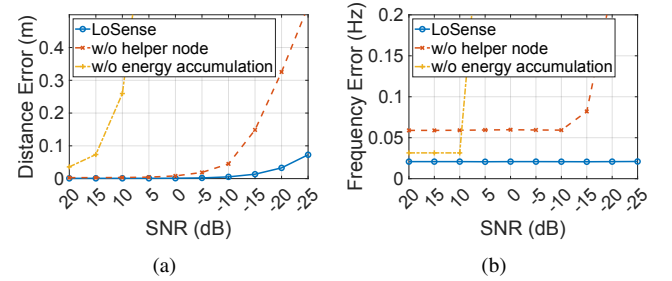

Fig. 12. Tracking errors for component-level evaluation with three different system implementations and various SNRs.

(2) LoSense W/O energy accumulation: In this setting, we skip the energy accumulation and perform circle fitting with all original signal samples.

We conduct the experiment over various SNR conditions. For each SNR setting, we make the transmitter send 20 LoRa packets. Then, at the receiver, we add white Gaussian noise to the received signal to generate signal copies of different SNRs,

i.e., from 20 dB to -15 dB with a step of 5 dB. The default SF is 12 and bandwidth is 125 kHz for all LoRa packets.

Results: Figure 12(a) shows the distance tracking accuracy of three implementations under various SNR conditions. The implementation without the helper node shows significant performance degradation compared with the native *LoSense*, whose distance tracking error reaches over 0.5m when the SNR is as high as 5 dB. This is due to the lack of phase feature amplification when there is no signal from the helper node. The small signal phase difference at the two receiving antennas is prone to be submerged by noises in low-SNR situations. The implementation without energy accumulation also shows performance degradation as the SNR decreases. Its distance tracking error raises sharply when the SNR goes below 0 dB, showing the energy accumulation significantly improve the combating noise ability of *LoSense*.

Figure 12(b) shows the frequency tracking errors of the three implementations. Only the full implementation can achieve accurate frequency tracking when SNR < 0 dB. The implementation without energy accumulation failed to track the vibration when SNR < 0 dB, indicating that the distance estimation in Figure 12(a) when SNR < 10 dB is meaningless. Even when SNR ≥ 10 dB, the error of the implementation without energy accumulation is much larger than *LoSense*. This is because, without energy accumulation, the original signals are too noisy to fit in a correct circle.

C. Field Experiment

Experiment setting: This experiment evaluates the performance of *LoSense* in outdoor field scenarios. We deploy both the LoRa transmitters and the receiver in an outdoor playground. The bird view of the experiment area is shown in Figure 11(a). The maximum range between the transmitter and the receiver is over 150m. We fix the position of receiver and move the transmitter to ten different position (i.e., P1 to P10 as shown in Figure 11(a)). We set transmitters to deliver LoRa packets with the data rate configuration of SF12 and the bandwidth of 125 kHz. The reciprocating linear actuator is used for providing transmitter motions at each position with the same configuration as described in Sec. VII. At each evaluated position, we make the transmitter send 20 LoRa packets. We estimate the averaged distance tracking errors and frequency errors at each position.

Results: The results for the field experiment are shown in Figure 11. We plot the tracked distance range for each position in Figure 11(b), where the maximum distance error of *LoSense* is lower than $2.32cm$ (at position P8). 50% of experiments have the error lower than $0.58cm$. We observe that the tracking accuracy is stable even when the transmitter is over one hundred meters away from the transmitter (i.e., at P6 to P10). This is because *LoSense* has the combating noise designs, such as energy accumulation and outliers elimination, which improves its performance for processing low-SNR signals in far fields. For the frequency tracking, the maximum frequency error of *LoSense* is lower than 0.089 Hz (on position P10). These
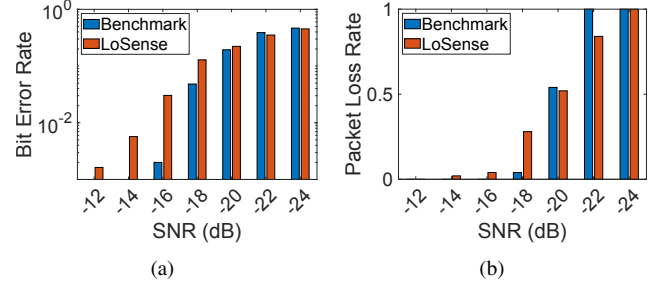

Fig. 13. BER and PLR performance of standard LoRa and *LoSense* under various SNRs.

results show that *LoSense* can achieve accurate frequency tracking in outdoor scenarios.

D. Impact on LoRa Communication

Experiment setting: This experiment verifies the impact of *LoSense* on LoRa communication. To measure how much the tracking process affects the alongside LoRa communication, we decode LoRa packets in the indoor experiments in Section VII-A. We set up a benchmark system where a moving transmitter sends LoRa packets to a fixed receiver. The SF and bandwidth are set to 9 and 250 kHz, respectively. Both the benchmark system and *LoSense* send LoRa packets for 50 times. We decode LoRa packets and compare the bit error rate (BER) and packet loss rate (PLR) for both *LoSense* and the benchmark system. A LoRa packet is considered lost when its bit error rate reaches 15%.

Results: Figure 13 shows the BER and PLR of *LoSense* and the benchmark system. Both the BER and PLR of these two systems increase as SNR decreases. The BER of *LoSense* increases faster than the benchmark when the SNR decreases from $-10dB$ to $-20dB$. This is because *LoSense* requires a helper node for concurrent transmission, which introduces higher interference for data communication. However, as LoRa CSS modulation is native robust against in-band interferences, *LoSense* still achieves reliable communication even when the SNR is as low as -16dB. When SNR ≥ $-16dB$, the BER of *LoSense* is lower than 3.0% and the PLR is only 4%, which is sufficient for providing reliable long-range communication in most IoT applications as the standard LoRa.

VIII. RELATED WORKS

A. LoRa ISAC

Integrated sensing and communication (ISAC) has attracted increasing interests from both academia and industrial for recent years. It is promising to integrate the data communication and wireless sensing into a single system for saving the scarce radio spectrum. Inspired by this idea, ReMix [24] uses the backscatter signal to enable data communication and wireless localization at the same time for in-body IoT devices. FullBreath [25], SignFi [26] and WiMU [27] sense human activities, e.g., walking, talking, breathing, with ongoing Wi-Fi data packet transmissions. LoRadar [17] modifies the FMCW radar and enables it to send LoRa signals, and hence the

radar can communicate with LoRa nodes as well as sensing. Different from previous research, *LoSense* uses signals from commodity LoRa transmitters for simultaneous sensing and communication in long range.

B. LoRa based Localization and Tracking

Previous works propose LoRa localization based on Received Signal Strength Indicator (RSSI) [8], [9], [28]–[30]. Since LoRa can support several or tens of kilometers communication, these systems can deploy a small number of LoRa gateways to cover a large area. For example, Choi et al [12] use RSSI fingerprints to localize LoRa nodes with only 4 LoRa gateways covering a $340m \times 340m$ area. The fingerprint map is generated by RSSI measured at different LoRa gateways, and stored in a database for future queries. Therefore, the localization/tracking error lies in the order of magnitude of tens of meters. These works have localization errors of hundreds of meters, due to the unstable measurement of RSSI in long-range dynamic environments. SateLoc [29] characterizes the channel attenuation property based on satellite images, and reduces the localization error to $50m$. Other works propose schemes to localizing LoRa transmitters based on Time Difference of Arrival (TDoA) [6], [7], [31]. Those schemes have to solve the challenge of asynchronous clock sources of multiple receivers, which introduces fluctuations in timestamps and further impacts the localization accuracy.

Research works present target sensing with LoRa signals [11], [13], [32], [33], which extract phase features from reflected signals for heartbeat or breath tracking. [14] tracks human activities, such as walking, waving, and breathing, with a sensing range of only tens of meters, due to the high attention of reflected LoRa signals. Previous works require dedicated signals and do not support simultaneous sensing and communication.

IX. Discussion

Scalability. *LoSense* can be easily applied in large-scale LoRa systems as it uses normal data communication signals for wireless sensing. Unlike previous LoRa tracking systems that requires LoRa nodes to transmit specialized signals for sensing, *LoSense* works completely at the same time as normal LoRa communication, only incurring additional complexity at the gateway. *LoSense* uses idle nodes as the helper transmitter for feature amplification, and thus incurs little burden for normal network operation. Besides, we leverage the global viewing of the LoRa gateway to find helper nodes with more energy and schedule them to help track the target. Thus, we can achieve the energy-consumption balance across the whole LoRa network.

Power Consumptions. We optimize the power consumption of *LoSense* in two ways: First, we avoid hardware and software modifications on target transmitters. Thus, the node-side power consumption is not increased. We put most computations at the receiver side (i.e., LoRa gateways) which has wall-plugged power supplies and can afford high computation overheads. Second, we schedule helper nodes based on the global view

of the centralized gateway to balance the power-consumption among different transmitters.

Multi-Targets Tracking. For concurrent LoRa transmissions with different configurations, e.g., different SFs or BWs, their signals are naturally orthogonal, and thus the receiver can easily separate the concurrent packets and track each node with interference. Otherwise, if multiple LoRa nodes with the same configuration transmit simultaneously, *LoSense* has first to separate collision signals. Previous literatures [34]–[36] show many approaches for decompose overlapped LoRa packets based on time and frequency features of concurrent LoRa signals. Besides, we can also integrate other sensors into the tracking method to help improve the accuracy [37]. Tracking multiple targets with the same LoRa configuration will be our future work.

X. Conclusion

In this paper, we propose *LoSense*, a system for integrated sensing and communication with LoRa signals. *LoSense* enables long-range movement tracking for active devices in the period of a regular LoRa packet transmission. We propose tracking models for active transmitters, and we design feature amplification and signal enhancement strategies for combating the noise and interference in LoRa signals. We apply dual antennas at the receiver to address the synchronization problem, and amplify the movement-induced phase variation by introducing a helper node. We implement *LoSense* with LoRa transmitters and USRP receivers, and extensively evaluate its performance in both indoor and outdoor scenarios. The evaluation results show that *LoSense* can achieve high-precise tracking with the accuracy of 3.38 cm in distance and 0.02 Hz in frequency even when the SNR is under -20 dB. *LoSense* also achieves long-range tracking in outdoor scenarios with distance errors less than 2.32 cm when the transmitter is 150 m apart from the receiver.

XI. Acknowledgements

References

[1] "Lora applications." https://www.semtech.com/lora/lora-applications/smart-agriculture.

[2] "Lora applications." https://www.semtech.com/lora/lora-applications/smart-industrial-control.

[3] "Lora applications." https://www.semtech.com/lora/lora-applications/smart-supply-chain-logistics.

[4] "Lorawan - what is it? a technical overview of lora and lorawan." https://lora-alliance.org/wp-content/uploads/2020/11/what-is-lorawan.pdf.

[5] M. Aernouts, N. BniLam, R. Berkvens, and M. Weyn, "TDAoA: A combination of TDoA and AoA localization with LoRaWAN," *Internet of Things*, vol. 11, p. 100236, 2020.

[6] D. Plets, N. Podevijn, J. Trogh, L. Martens, and W. Joseph, "Experimental Performance Evaluation of Outdoor TDoA and RSS Positioning in a Public LoRa Network," in *2018 International Conference on Indoor Positioning and Indoor Navigation (IPIN)*. Nantes: IEEE, 2018, pp. 1–8.

[7] N. Podevijn, D. Plets, J. Trogh, L. Martens, P. Suanet, K. Hendrikse, and W. Joseph, "TDoA-Based Outdoor Positioning with Tracking Algorithm in a Public LoRa Network," *Wireless Communications and Mobile Computing*, vol. 2018, pp. 1–9, 2018.

[8] K.-H. Lam, C.-C. Cheung, and W.-C. Lee, "RSSI-Based LoRa Localization Systems for Large-Scale Indoor and Outdoor Environments," *IEEE Transactions on Vehicular Technology*, vol. 68, no. 12, pp. 11 778–11 791, 2019.

[9] ——, "New RSSI-Based LoRa Localization Algorithms for Very Noisy Outdoor Environment," in *2018 IEEE 42nd Annual Computer Software and Applications Conference (COMPSAC)*. Tokyo, Japan: IEEE, 2018, pp. 794–799.

[10] J. Liu, J. Gao, S. Jha, and W. Hu, "Seirios: Leveraging multiple channels for LoRaWAN indoor and outdoor localization," in *Proceedings of the 27th Annual International Conference on Mobile Computing and Networking*. New Orleans Louisiana: ACM, 2021, pp. 656–669.

[11] A. Bansal, A. Gadre, V. Singh, A. Rowe, B. Iannucci, and S. Kumar, "OwLL: Accurate LoRa Localization using the TV Whitespaces," in *Proceedings of the 20th International Conference on Information Processing in Sensor Networks (Co-Located with CPS-IoT Week 2021)*. Nashville TN USA: ACM, 2021, pp. 148–162.

[12] W. Choi, Y.-S. Chang, Y. Jung, and J. Song, "Low-Power LoRa Signal-Based Outdoor Positioning Using Fingerprint Algorithm," *ISPRS International Journal of Geo-Information*, vol. 7, no. 11, p. 440, 2018.

[13] B. Xie and J. Xiong, "Combating interference for long range LoRa sensing," in *Proceedings of the 18th Conference on Embedded Networked Sensor Systems*. Virtual Event Japan: ACM, 2020, pp. 69–81.

[14] F. Zhang, Z. Chang, K. Niu, J. Xiong, B. Jin, Q. Lv, and D. Zhang, "Exploring LoRa for Long-range Through-wall Sensing," *Proceedings of the ACM on Interactive, Mobile, Wearable and Ubiquitous Technologies*, vol. 4, no. 2, pp. 1–27, 2020.

[15] H. Jiang, J. Zhang, X. Guo, and Y. He, "Sense Me on the Ride: Accurate Mobile Sensing over a LoRa Backscatter Channel," in *Proceedings of the 19th ACM Conference on Embedded Networked Sensor Systems*. Coimbra Portugal: ACM, 2021, pp. 125–137.

[16] Y. Wang, X. Zheng, L. Liu, and H. Ma, "PolarTracker: Attitude-aware Channel Access for Floating Low Power Wide Area Networks," in *IEEE INFOCOM 2021 - IEEE Conference on Computer Communications*. IEEE, pp. 1–10. [Online]. Available: https://ieeexplore.ieee.org/document/9488714/

[17] Q. Huang, Z. Luo, J. Zhang, W. Wang, and Q. Zhang, "LoRadar: Enabling Concurrent Radar Sensing and LoRa Communication," vol. 21, no. 6, pp. 2045–2057. [Online]. Available: https://ieeexplore.ieee.org/document/9248648/

[18] L. K. Baghel, S. Gautam, V. K. Malav, and S. Kumar, "TEMPSENSE: LoRa Enabled Integrated Sensing and Localization Solution for Water Quality Monitoring," vol. 71, pp. 1–11. [Online]. Available: https://ieeexplore.ieee.org/document/9774415/

[19] "Mobius transformation," https://en.wikipedia.org/wiki/Mobius_transformation.

[20] Y. Zhang, J. Wang, W. Wang, Z. Wang, and Y. Liu, "Vernier: Accurate and Fast Acoustic Motion Tracking Using Mobile Devices," in *IEEE INFOCOM 2018 - IEEE Conference on Computer Communications*. IEEE, pp. 1709–1717. [Online]. Available: https://ieeexplore.ieee.org/document/8486365/

[21] "Matlab function nlinfit," https://www.mathworks.com/help/stats/nlinfit.html.

[22] "Semtech sx1276 datasheet." https://www.semtech.com/products/wireless-rf/lora-core/sx1276.

[23] "Gnu radio library," https://www.gnuradio.org/.

[24] D. Vasisht, G. Zhang, O. Abari, H.-M. Lu, J. Flanz, and D. Katabi, "In-body backscatter communication and localization," in *Proceedings of the 2018 Conference of the ACM Special Interest Group on Data Communication*. ACM, pp. 132–146. [Online]. Available: https://dl.acm.org/doi/10.1145/3230543.3230565

[25] Y. Zeng, D. Wu, R. Gao, T. Gu, and D. Zhang, "FullBreathe: Full Human Respiration Detection Exploiting Complementarity of CSI Phase and Amplitude of WiFi Signals," vol. 2, no. 3, pp. 1–19. [Online]. Available: https://dl.acm.org/doi/10.1145/3264958

[26] Y. Ma, G. Zhou, S. Wang, H. Zhao, and W. Jung, "SignFi: Sign Language Recognition Using WiFi," vol. 2, no. 1, pp. 1–21. [Online]. Available: https://dl.acm.org/doi/10.1145/3191755

[27] R. H. Venkatnarayan, G. Page, and M. Shahzad, "Multi-User Gesture Recognition Using WiFi," in *Proceedings of the 16th Annual International Conference on Mobile Systems, Applications, and Services*. ACM, pp. 401–413. [Online]. Available: https://dl.acm.org/doi/10.1145/3210240.3210335

[28] B. Islam, M. T. Islam, J. Kaur, and S. Nirjon, "LoRaIn: Making a Case for LoRa in Indoor Localization," in *2019 IEEE International Conference on Pervasive Computing and Communications Workshops (PerCom Workshops)*. Kyoto, Japan: IEEE, 2019, pp. 423–426.

[29] Y. Lin, W. Dong, Y. Gao, and T. Gu, "SateLoc: A Virtual Fingerprinting Approach to Outdoor LoRa Localization using Satellite Images," in *2020 19th ACM/IEEE International Conference on Information Processing in Sensor Networks (IPSN)*. Sydney, NSW, Australia: IEEE, 2020, pp. 13–24.

[30] C. Sanchez, B. Arpi, A. Vazquez-Rodas, F. Astudillo-Salinas, and L. I. Minchala, "Performance Evaluation of RSSI-based Positioning System with Low-cost LoRa Devices," in *Proceedings of the 16th ACM International Symposium on Performance Evaluation of Wireless Ad Hoc, Sensor, & Ubiquitous Networks - PE-WASUN '19*. Miami Beach, FL, USA: ACM Press, 2019, pp. 37–44.

[31] B. C. Fargas and M. N. Petersen, "GPS-free geolocation using LoRa in low-power WANs," in *2017 Global Internet of Things Summit (GIoTS)*. Geneva, Switzerland: IEEE, 2017, pp. 1–6.

[32] F. Zhang, Z. Chang, J. Xiong, R. Zheng, J. Ma, K. Niu, B. Jin, and D. Zhang, "Unlocking the Beamforming Potential of LoRa for Long-range Multi-target Respiration Sensing," vol. 5, no. 2, pp. 1–25. [Online]. Available: https://dl.acm.org/doi/10.1145/3463526

[33] J. Jiang, J. Wang, Y. Chen, Y. Liu, and Y. Liu, "Locra: Enable practical long-range backscatter localization for low-cost tags," 2023.

[34] S. Tong, Z. Xu, and J. Wang, "CoLoRa: Enabling Multi-Packet Reception in LoRa," in *IEEE INFOCOM 2020 - IEEE Conference on Computer Communications*. Toronto, ON, Canada: IEEE, 2020, pp. 2303–2311.

[35] X. Wang, L. Kong, L. He, and G. Chen, "mLoRa: A Multi-Packet Reception Protocol in LoRa networks," in *2019 IEEE 27th International Conference on Network Protocols (ICNP)*. Chicago, IL, USA: IEEE, 2019, pp. 1–11.

[36] S. Tong, J. Wang, and Y. Liu, "Combating packet collisions using non-stationary signal scaling in LPWANs," in *Proceedings of the 18th International Conference on Mobile Systems, Applications, and Services*. ACM, pp. 234–246. [Online]. Available: https://dl.acm.org/doi/10.1145/3386901.3388913

[37] Q. Shi, S. Zhao, M. Lu, M. Jia, and X. Cui, "Anchor self-localization algorithm based on uwb ranging and inertial measurements," *Tsinghua Science and Technology*, vol. 24, no. 6, pp. 728–737, 2019. [Online]. Available: https://www.sciopen.com/article/10.26599/TST.2018.9010102